Article

INTERNATIONAL JOURNAL OF DAMAGE MECHANICS

International Journal of Damage Mechanics
0(0) 1–28

DOI: 10.1177/1056789518775173
journals.sagepub.com/home/ijd

SAGE

Damage mechanics-based approach to studying effects of overload on fatigue life of notched specimens

Jiawei Huang[1], Qingchun Meng[1], Zhixin Zhan[1,2], Weiping Hu[1] and Fei Shen[2]

Abstract

A continuum damage mechanics-based method is adopted to predict the fatigue life of notched specimens subjected to constant amplitude cyclic loading while containing single or multiple overloads. The residual stress and plastic damage induced by an overload are considered to be the main factors affecting the fatigue life of a specimen. The residual stress and plastic strain fields of a notched specimen are calculated using the elastic–plastic finite element method. The mean stress of the following cyclic loading is then varied by superimposing the residual stress. Meanwhile, the plastic damage is calculated based on the ductile damage model and accumulated into the total damage of the material. The quantitative effects of an overload on the damage evolution and the fatigue life are evaluated. Furthermore, the effects of the damage–overload ratio on the variation of the residual stress induced by an overload are investigated, and the effects of the occurrence time for a single overload and the occurrence frequency for multiple overloads are studied.

Keywords

Damage mechanics, fatigue life, overload, residual stress, notched specimens

Introduction

Fatigue failure is the most common failure mode for mechanical components subjected to cyclic loading. Therefore, a prediction of the fatigue life of a structure and the factors influencing such fatigue life has received significant attention. Many types of methods have been developed to deal

[1]School of Aeronautic Science and Engineering, Beihang University, Beijing, China
[2]School of Mechanical and Aerospace Engineering, Nanyang Technological University, Singapore

Corresponding author:
Zhixin Zhan, School of Aeronautic Science and Engineering, Beihang University, Room D604, New Main Building, 37th Xueyuan Road, Beijing 100191, China.
Email: zzxupc@163.com

with the fatigue problems. Among these methods, recently, damage mechanics-based approaches (Darban et al., 2014; Lv et al., 2015; Sun et al., 2017; Zghal et al., 2016) have become the important solutions to analyse the fatigue damage of practical structures.

Practical structures are usually not smooth; instead, holes, grooves or notches, as well as variable cross sections, are generally involved. These geometrical features can induce a stress concentration (Castro et al., 2016), and the stress concentration zone is always the critical zone with regard to fatigue. To study the effects of different geometrical features, many fatigue tests have been conducted on notched specimens (Shen et al., 2015), which have proved to be an effective test method. On the other hand, considering that a structure is not always subjected to a constant amplitude (CA) cyclic loading and that an overload probably occurs either occasionally or regularly, it is necessary to conduct fatigue tests for notched specimens that have experienced an overload. In general, an overload can bring about a local plastic strain and residual stress to a notched specimen, thereby affecting its fatigue life. Therefore, many studies have discussed the effects of overloading from the aspects of plastic strain and residual stress.

To evaluate the effects of residual stress, we first need to determine the residual stress field induced by an overload. With this regard, experiments are typically adopted. Dalaei and Karlsson (2011) used an X-ray diffraction technique to measure the residual stress, and discussed the influence of an overload on the stability of residual stresses in shot-peened normalized steel. In addition, the relaxation of the residual stress was also analysed. In addition to experiments, finite element methods are also widely used. Xiao et al. (2014) used the finite element method combined with Suresh's model (Suresh and Giannakopoulos, 1998) to simulate the residual stress distribution near a crack tip. The predicted result was in good agreement with the experiment data obtained from an instrumented indentation test. Chengqing et al. (2013) adopted a linear elastic unloading assumption to predict the residual stress using finite element methods and obtained highly accurate results. However, the unloading after an overload may cause reverse yielding, which cannot be treated as linear elastic unloading. Smith et al. (2012) conducted a prediction of residual stress in stainless steel welds by introducing a Lemaitre–Chaboche mixed hardening model into the finite element method. The predicted residual stress was consistent with the experiment results. Overall, a numerical calculation is an effective method to obtain the residual stress field induced through an overload. The effect of residual stress on the fatigue life is typically reflected through variation in the mean stress. However, the residual stress may relax during the following cyclic loading, which needs to be carefully studied.

In addition to residual stress, plastic damage is also introduced through an overload owing to the occurrence of plastic strain around the notch tip. In general, a proper overload does increase the fatigue life, whereas if the overload is too high, plastic damage will clearly appear around the notch tip, which could decrease the fatigue life. Therefore, it is necessary to quantitatively evaluate the effects of plastic damage.

At present, studies on the effects of an overload have mainly focused on an improvement of the fatigue crack propagation life. Sander and Richard (2005) found that overload does increase the fatigue life, but different types of overload affect the fatigue life at different levels. Ramos et al. (2003) studied the effects of single and multiple overloads on the fatigue life and noticed that two equal and consecutive overloads lead to a longer fatigue life than a single peak overload. Sarkheil and Foumani (2014) used Walker's equation (Walker, 1970) with a generalized Willenborg model (Gallagher, 1974) to study the crack growth retardation owing to periodic tensile overloads. The results showed that, under the same CA loading, the relationship between the optimum overload ratio and the overload occurrence frequency is linear at a semi-log scale. With regard to the effects of an overload on the fatigue crack initiation life, few studies have been reported. Theil (2016)

proposed an empirical prediction method based on an S/N curve for the fatigue crack initiation life of a structure/specimen, which can take into account the effects of an overload. The predicted results were better than those obtained using the Palmgren–Miner rule (Kauzlarich, 1989). However, the results were seriously overestimated for certain cases. Zuo et al. (2015) found that for variable amplitude loading, the load sequence has considerable effect on fatigue life. He then presented the fatigue driving stress that causes fatigue damage to take the effects of load history into consideration. The predicted fatigue life obtained by his method is in a good agreement with experiment results. In addition, the method proposed for the investigation of the effect of variable amplitude loading (Zuo et al., 2015) can also be applied to study the effect of overload, owing to the overload may be regarded as a special variable amplitude load.

In this study, the effects of overloading are investigated through a damage mechanics-based approach. A damage-coupled elasto-plastic constitutive model is employed to describe the mechanical behaviours of a material experiencing an overload and cyclic loading. Plastic damage induced by an overload is calculated using Lemaitre's ductile damage model. The residual stress caused by an overload is superimposed with the cyclic loading to account for the following fatigue damage. Two different fatigue damage models, a stress-based model and a plastic-strain based model, are adopted to calculate the damage evolution of the material. The numerical implementations of these two damage models are introduced into ABAQUS using the UMAT subroutine. The effects of plastic damage and residual stress caused by an overload are quantitatively evaluated. The predicted fatigue life is compared with the experiment data. The influencing factors, including the overload ratio, the occurrence time for a single overload case and the occurrence frequency for a multiple overload case, are all analysed in detail. In addition, the relaxation of the residual stress during cyclic loading is investigated.

Theoretic models

Damage-coupled elasto-plastic constitutive model

Damage in a mechanical sense is the creation and growth of micro-cracks and micro-voids (Lemaître, 1992). In engineering, the mechanics of continuous media can be described using a representative volume element (RVE). Lemaitre proposed some fundamental concepts (Lemaître, 1992) regarding damage mechanics. For the case of isotropic damage in isotropic materials, the scalar damage variable D is defined as

$$D = \frac{S_D}{S} \tag{1}$$

$$S = S_E + S_D \tag{2}$$

where S is the area of the section in the RVE, S_D is the total area of damage and S_E is the effective area.

The effective stress $\tilde{\sigma}$ is used to describe the stress over the effective area of a section:

$$\tilde{\sigma} = \frac{P}{S_E} = \frac{P}{(1-D)S} = \frac{\sigma}{1-D} \tag{3}$$

where P is the load applied to the section.

Based on the hypothesis of strain equivalence, damage extent D can be expressed through the deterioration of stiffness:

$$D = \frac{E - E_D}{E} \tag{4}$$

where E is the initial Young's modulus of RVE, and E_D is the equivalent Young's modulus of the damaged RVE.

In this paper, the elasto-plastic constitutive model (Chaboche, 1986, 1989, 2008) proposed by Chaboche is adopted. This model has been extended to consider the kinematic hardening (Abdel-Karim, 2009, 2010; Chaboche, 1991) and is capable of describing the cyclic deformation behaviour well. In addition, considering the material damage, the fundamental concept of continuum damage mechanics needs to be introduced into the model.

First, considering a small deformation, the total strain ε_{ij} can be decomposed as:

$$\varepsilon_{ij} = \varepsilon_{ij}^e + \varepsilon_{ij}^p \tag{5}$$

where ε_{ij}^e is the elastic strain, and ε_{ij}^p is the plastic strain.

The damage coupled elastic constitutive equation takes the following form:

$$\varepsilon_{ij}^e = \frac{1+v}{E}\left(\frac{\sigma_{ij}}{1-D}\right) - \frac{v}{E}\left(\frac{\sigma_{kk}\delta_{ij}}{1-D}\right) \tag{6}$$

where v is the Poisson's ratio, σ_{ij} is the Cauchy stress and δ_{ij} is the Kronecker delta: $\delta_{ij} = \begin{cases} 0, & \text{if } i \neq j \\ 1, & \text{if } i = j \end{cases}$. The subscripts i and j vary from 1 to 3.

The von Mises yield function, hardening law and plastic flow with damage are given as (Lemaître, 1992):

$$f = \sigma_{eq} - R \tag{7}$$

$$\sigma_{eq} = \left(\frac{\sigma_{ij}}{1-D} - x_{ij}\right)_{eq} \tag{8}$$

$$\dot{\varepsilon}_{ij}^p = \dot{\lambda}\frac{\partial f}{\partial \sigma_{ij}} = \frac{3}{2}\frac{\dot{\lambda}}{1-D}\frac{\left(\frac{\sigma_{ij}}{1-D} - x_{ij}\right)_{dev}}{\left(\frac{\sigma_{kl}}{1-D} - x_{kl}\right)_{eq}} \tag{9}$$

$$\dot{r} = \sqrt{\frac{2}{3}\dot{\varepsilon}_{ij}^p\dot{\varepsilon}_{ij}^p} = \frac{\dot{\lambda}}{1-D} \tag{10}$$

$$x_{ij} = \sum_{k=1}^{3} x_{ij}^{(k)} \tag{11}$$

$$x_{ij}^{(\dot{k})} = (1-D)\left(\frac{2}{3}C^{(k)}\varepsilon_{ij}^{\dot{p}} - \gamma^{(k)}x_{ij}^{(k)}\dot{r}\right) \tag{12}$$

$$\dot{R} = (1-D)b(Q-R)\dot{r} \tag{13}$$

where the subscript *dev* represents the deviatoric part of the stress, *eq* is the von Mises equivalent stress, x_{ij} is the deviatoric part of the back stress, R is the size of the yield surface, $\dot{\lambda}$ is the plastic multiplier and $\dot{r}$ is the accumulated plastic strain rate. In this study, three groups of back stress are used to fit the stress–strain curve. Material constants $C^{(k)}, \gamma^{(k)}, Q$ and b can be determined experimentally.

Fatigue damage evolution models

Generally, the damage of material can be calculated employing stress-based model or plastic–strain based model depending on the loading level. If the loading level is not high and only elastic deformation occurs, the stress-based model is adopted. This case conventionally corresponds to the high-cycle fatigue. Meanwhile, if the loading level is enough high that the obvious plastic deformation can be observed, the plastic–strain based model ought to be used and the elastic damage can be completely ignored. This case is typically related to the low-cycle fatigue. However, for some cases, plastic deformation is not much significant, instead, its order is comparative to that of elastic deformation. Consequently, in this scenario, the damage is determined by taking the maximum value between elastic damage and plastic damage, the method adopted in Shen et al. (2015), in which predicted fatigue life agrees well with experiment results.

When there is no increment of plastic strain within a loading cycle, the damage increment is mainly determined based on the state of the stress. For the uniaxial case, the damage evolution equation proposed by Lemaitre et al. (1993) is expressed as follows:

$$\frac{dD_e}{dN} = \left[1-(1-D)^{\beta+1}\right]^{1-a\left[\frac{\sigma_a-\sigma_{l0}(1-b_1\sigma_m)}{\sigma_u-\sigma_{max}}\right]} \times \left[\frac{\sigma_{\max}-\sigma_m}{M_0(1-b_2\sigma_m)(1-D)}\right]^{\beta} \tag{14}$$

where σ_a, σ_m and σ_{max} are the stress amplitude, mean stress and maximum equivalent stress during the loading cycle, respectively. σ_{l0} indicates the fatigue limit of smooth specimen under fully reversed loading conditions. Generally, for engineering materials, including aluminum alloys, the fatigue limit is the cyclic stress level below which a fatigue failure does not occur in material which undergoes the specified number of cycles, usually 10^7. According to the Military Handbook-MIL-HDBK-5H (1998), the fatigue limit σ_{l0} of 7075-T6 aluminum alloy is 117 MPa. σ_u is the ultimate tensile stress, and D_e is the elastic damage. The parameters b_1, b_2, β, M_0 and a can be determined from equation (14) using the fatigue test data of a standard specimen. The details of this are presented in Parameter calibration in damage evolution models section.

For a multi-axial case, equation (14) has been extended from Chaudonneret (1993), who developed the following:

$$\frac{dD_e}{dN} = \left[1-(1-D)^{\beta+1}\right]^{1-a\left[\frac{A_{II}-\sigma_{l0}\left(1-3b_1\sigma_{H,mean}\right)}{\sigma_u-\sigma_{eq,max}}\right]} \times \left[\frac{A_{II}}{M_0\left(1-3b_2\sigma_{H,mean}\right)(1-D)}\right]^{\beta} \tag{15}$$

$$A_{II} = \frac{1}{2}\left[\frac{3}{2}\left(S_{ij,max}-S_{ij,min}\right)\left(S_{ij,max}-S_{ij,min}\right)\right] \tag{16}$$

where A_{II} represents the amplitude of the octahedral shear stress, $S_{ij,max}$ is the maximum value, $S_{ij,min}$ is the minimum value of the deviatoric part of the stress, $\sigma_{eq,max}$ is the maximum equivalent stress over a loading cycle and $\sigma_{H,mean}$ is the mean value of the hydrostatic stress during a loading cycle.

Table 1. Parameters used in hardening law of Al 7075-T6.

Parameters	E	v	σ_y	Q	b	$\gamma^{(1)}, \gamma^{(2)}, \gamma^{(3)}$	$C^{(1)}, C^{(2)}, C^{(3)}$
Values	70 GPa	0.32	464 MPa	132.88 MPa	0.053	25.73, 43.36, 327.77	1019 MPa, 39.8 MPa, 6005.9 MPa

When an increment of plastic strain occurs within a loading cycle, the increment of fatigue damage is determined based on the accumulated plastic strain. The damage evolution law for the uniaxial stress case is given by (Lemaitre et al., 1993; Warhadpande et al., 2012)?

$$\frac{dD_p}{dN} = \left[\frac{(\sigma_{max})^2}{2ES(1-D)^2}\right]^m \left|\Delta\varepsilon_p\right| \tag{17}$$

where $\Delta\varepsilon_p$ is the increment in amplitude of the plastic cyclic strain during a loading cycle, D_p is the plastic damage and S and m are material parameters that can be obtained through experiment data (Military Handbook-MIL-HDBK-5H, 1998). The determination of these parameters is presented in Parameter calibration in damage evolution models section.

For the multi-axial case, the strain-controlled damage evolution is written as

$$\frac{dD_p}{dN} = \left[\frac{(\sigma^*_{max})^2}{2ES(1-D)^2}\right]^m \Delta r \tag{18}$$

where σ^*_{max} and Δr are the maximum equivalent stress and the increment in amplitude of the plastic strain during a loading cycle.

It should be noted that the variable D in equations (1)–(13) represents the damage of material whatever form it is determined as. The variables D_e and D_p in equations (14) and (17) are the specific expressions corresponding to the different models.

Material and parameter calibration

In this paper, 7075-T6 aluminium alloy is studied. The basic mechanical properties of the material (Military Handbook-MIL-HDBK-5H, 1998) are listed in Table 1. In addition to these parameters, two other types of material parameters need to be calibrated: (i) material parameters in the elastic–plastic constitutive model and (ii) material parameters in the damage evolution models including the stress-based elastic damage model and plastic–strain based plastic damage model. The following sections describe the parameter calibration in detail.

Parameter calibration in the elastic–plastic constitutive model

As shown in Figure 1, the stress–plastic strain curve of the uniaxial tensile test is used to calibrate the material parameters in the hardening law. In this study, both isotropic hardening and nonlinear kinematic hardening are considered. The stress–plastic strain relationship can be expressed as follows:

$$\sigma = \sigma_y + \sum_{k=1}^{3} p_k\left(1 - e^{-t_k\varepsilon_p}\right) + p_4\left(1 - e^{-t_4\varepsilon_p}\right) \tag{19}$$

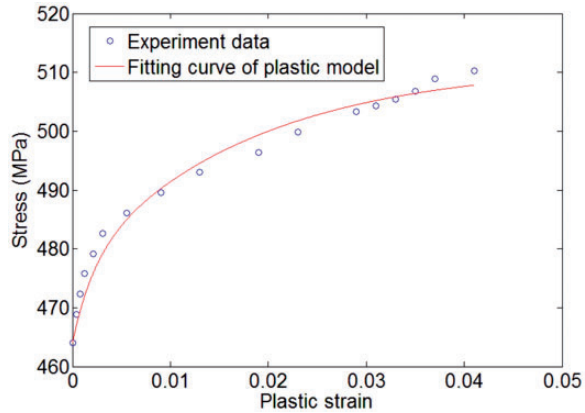

Figure 1. Experiment data (Military Handbook-MIL-HDBK-5H, 1998) and fitted stress–strain curve.

where σ_y represents the initial yield stress, and three components of back stress are employed to fit the experiment data. The parameters $C^{(k)}, \gamma^{(k)}, Q$ and b in equations (12) and (13) can be obtained using p_k and t_k as follows.

$$C^{(k)} = p_k t_k \tag{20}$$

$$\gamma^{(k)} = t_k \tag{21}$$

$$Q = p_4 \tag{22}$$

$$b = t_4 \tag{23}$$

The calibrated material parameters are listed in Table 1. In addition, the fitted curve versus the experiment data (Military Handbook-MIL-HDBK-5H, 1998) is shown in Figure 1.

Parameter calibration in damage evolution models

Parameter calibration in stress-based damage model. Five parameters, a, M_0, β, b_1 and b_2, in the stress-based damage model need to be calibrated. First, by integrating equation (14) from $D=0$ to $D=1$, the fatigue life is obtained as follows:

$$N_F = \frac{1}{1+\beta}\frac{1}{aM_0^{-\beta}}\frac{\sigma_u - \sigma_{max}}{(\sigma_a - \sigma_{l0}(1-b_1\sigma_m))}\left[\frac{\sigma_a}{1-b_2\sigma_m}\right]^{-\beta} \tag{24}$$

For the case of smooth specimens under uniaxial fatigue loading with stress ratio $R=-1$, equation (24) can be simplified as: $N_F = \frac{1}{1+\beta}\frac{1}{aM_0^{-\beta}}\frac{\sigma_u-\sigma_{max}}{(\sigma_a-\sigma_{l0})}(\sigma_a)^{-\beta}$. According to the stress-controlled high cycle fatigue test with $R=-1$ (Military Handbook-MIL-HDBK-5H, 1998), the experiment data of 18 specimens were used to calibrate the values of β and $aM_0^{-\beta}$ by employing least square method.

Parameters b_1 and b_2 are then determined from the experiment data (Military Handbook-MIL-HDBK-5H, 1998) at different mean stresses. Finally, a and M_0 are obtained using the damage-mechanics finite element method (Shen et al., 2015, 2016; Zhan et al., 2015a, 2015b). The calibrated parameters are listed in Table 2.

Parameter calibration in plastic strain-based damage evolution model. Two parameters, S and m, in the plastic strain-based damage model need to be calibrated. First, the stress–strain curve under cyclic loading can be described as follows:

$$\sigma_{max} = K'\left(\frac{\Delta\varepsilon_p}{2}\right)^{n'} \tag{25}$$

Then, for the case of a strain-controlled low cycle fatigue test, by integrating equation (17) from $D=0$ to $D=1$, and substituting equation (25), the fatigue life can be obtained as

$$N_F = \frac{1}{2(2m+1)}\left(\frac{2^{1+2n'}ES}{(K')^2}\right)^m (\Delta\varepsilon_p)^{-(1+2mn')} \tag{26}$$

where n' and K' are as obtained from a previous study (Dowling, 1993), and are shown in Table 3. Then, in order to obtain the parameter S and m, we used experiment data of strain-controlled low-cycle fatigue test (incremental step test) from Mil-HDBK-5 (Military Handbook-MIL-HDBK-5H, 1998). In the test, following the standard ASTM E606-12 (ASTM E606/E606M-12, 2012), smooth specimens of aluminum alloy sheet were used. The cyclic loading is axial, stress ratio R is -1 and the frequency is set between 5 Hz and 30 Hz so as to avoid increased resistance to axial stress influenced by restraints. The values of S and m are listed in Table 3.

Computational methodology

Finite element model

A notched specimen made of 7075-T6 is studied in this paper, which will be used for validation of the methods and a study of the influencing factors. The geometry of the specimen is illustrated

Table 2. Parameters of Al 7075-T6 for stress-controlled fatigue damage model.

Parameters	a	M_0	β	b_1	b_2
Values	0.75	2400	5.57	0.0014	0.0018

Table 3. Parameters of Al 7075-T6 for strain-controlled fatigue damage model.

Parameters	S	m	K'	n'
Values	2.90	7.62	977MPa	0.106

in Figure 2. The thickness of the specimen is 2.5 mm, and the stress concentration factor is 2.0. A remote tensile overload, followed by subsequent tension–compression cyclic loadings, was applied to the specimens. In the ABAQUS platform, only one-eighth of the model was built as shown in Figure 3, and symmetric boundary conditions were applied to the symmetric surfaces of the specimen. The element type is a C3D8, which is defined as a 3-D solid element including eight nodes with three degrees of freedom per node. A mesh convergence study was conducted to obtain the appropriate mesh size. The maximum von Mises stresses corresponding to the different mesh sizes under the same tensile load are listed in Table 4. The minimum element size of 0.088 mm $\times$0.098 mm $\times$0.156 mm was finally adopted for an additional finite element method simulation.

Residual stress computation

In this paper, a damage coupled Chaboche plastic model is used as the material model. The residual stress induced by an overload was obtained after the specimen was totally unloaded.

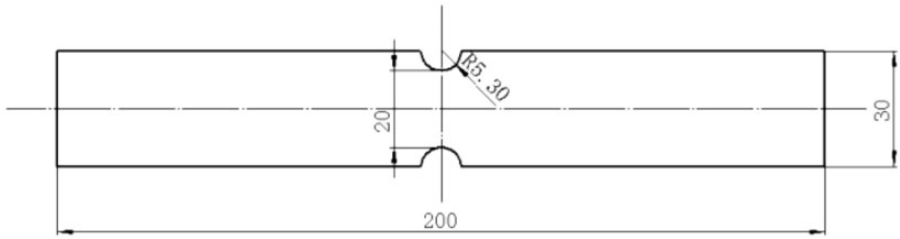

Figure 2. Geometry of notched specimen (dimensions in mm).

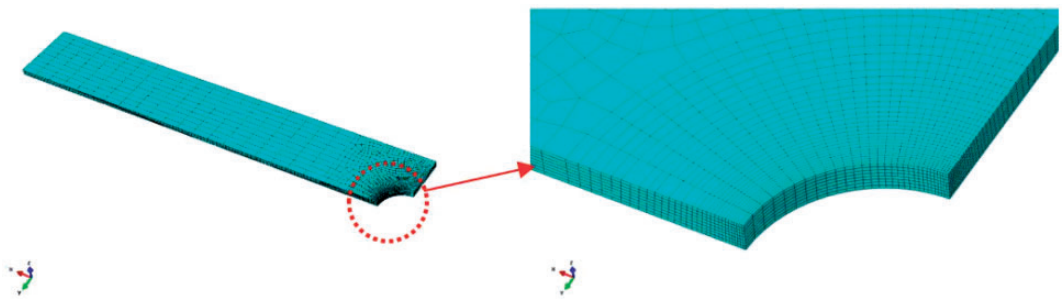

Figure 3. One-eighth model built in ABAQUS/CAE.

Table 4. Maximum von Mises stress corresponding to different mesh sizes.

	Mesh size 1	Mesh size 2	Mesh size 3
Minimum element size	0.102 mm $\times$0.132 mm $\times$0.178 mm	0.097 mm $\times$0.118 mm $\times$0.156 mm	0.088 mm $\times$0.098 mm $\times$0.156 mm
Stress/MPa	307.5	307.1	306.9

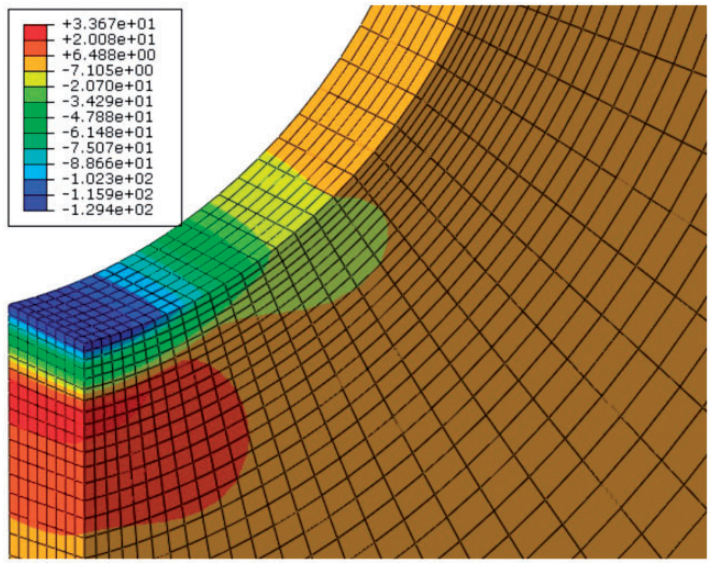

Figure 4. Longitudinal residual stress (MPa) distribution of specimen experiencing overload of 300 MPa.

An example of the residual stress distribution for the case of a notched specimen experiencing an overload of 300 MPa is shown in Figure 4. The maximum compressive residual stress appears at the tip of the notch, and the maximum compressive stress is about 129 MPa. A tensile residual stress zone is just below the compressive residual stress zone, with the maximum value of only 33.6 MPa.

When the fatigue load is applied to the specimen, the residual stress still remains and is obtained after each loading cycle. After the specimen shown in Figure 4 experienced 2000 cycles of fatigue loading with a maximum stress of 205.5 MPa following an overload of 300 MPa, the residual stress field was changed, which is shown in Figure 5. The maximum longitudinal compressive residual stress at the notch tip decreased from 129 MPa to 35.7 MPa, and the corresponding location also varied from the surface to the layer below the surface. The maximum tensile residual stress decreased from 33.6 MPa to 28.3 MPa as well. The effect of damage evolution on the variation of the residual stress is discussed in detail in Effects of damage on the variation of residual stress section.

Calculation of plastic damage induced by overload

The benefit of an overload for increasing the fatigue life of a notched specimen is mainly attributed to the introduction of a compressive residual stress. On the other hand, plastic damage is introduced simultaneously owing to the occurrence of plastic strain. Therefore, it is necessary to calculate the plastic damage to comprehensively evaluate the effect of an overload.

The damage induced by an overload can be considered as ductile damage considering that overload usually leads to plastic deformation at the root of notch. Consequently, a damage model describing the fatigue damage related to the plastic strain is adopted to calculate the plastic damage induced by an overload. According to the assumption proposed by Lemaitre and

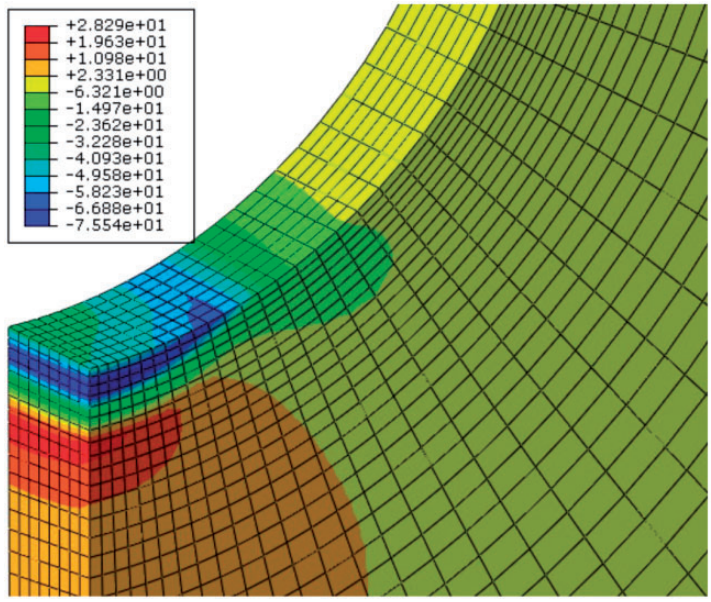

Figure 5. Longitudinal residual stress (MPa) distribution after $N = 2000$ loading cycles.

Desmorat (2005), i.e., $\frac{\sigma^*_{max}}{1-D} \approx \sigma_{eq,max} = const$, by integrating equation (17) along the loading history of the overload, the plastic damage D_0 induced by overload can be obtained as

$$D_0 = \frac{1}{2}\left[\frac{(\sigma_{eq,max})^2}{2ES}\right]^m |\varepsilon_p| \tag{27}$$

where $\sigma_{eq,max}$ and ε_p are the maximum von Mises stress and the maximum plastic strain within the overload history, respectively.

Figure 6 shows the calculated plastic damage field induced by an overload with a maximum value of 270 MPa. Theoretically, the damage along the thickness direction should be the same. However, a difference in damage along the thickness direction exists because of an unavoidable computational error. However, the difference is very small, and is quite acceptable.

The maximum amount of plastic damage occurs at the tip of the notch where the stress and plastic strain are both the largest. The plastic damage will be accumulated with the following fatigue damage, thereby affecting the fatigue life of the specimen, which is described in the next section.

Fatigue damage accumulation

According to the fatigue damage evolution model presented in Fatigue damage evolution models section, a flowchart of the numerical implementation of fatigue damage accumulation is shown in Figure 7, and the detailed steps of the calculation are as follows:

(1) Initialize all of the parameters.
(2) Calculate the stresses and strains of the specimen under cyclic loading and residual stress (if present).

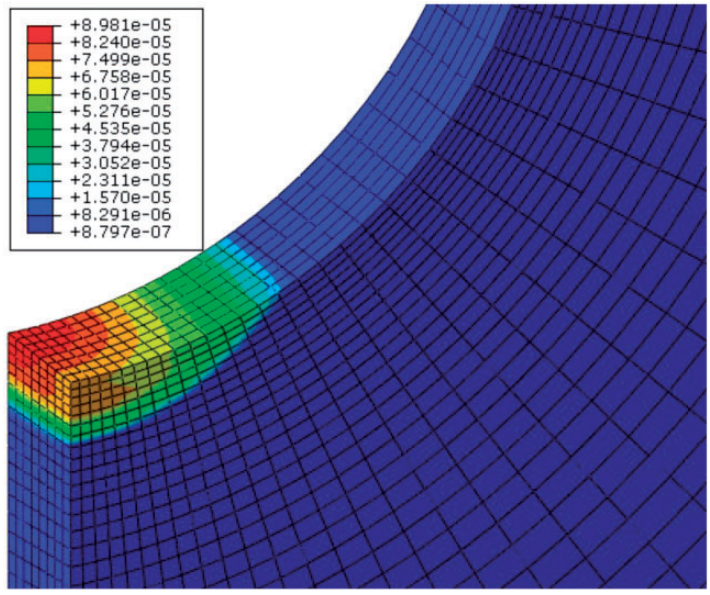

Figure 6. Initial plastic damage under an overload of 270 MPa.

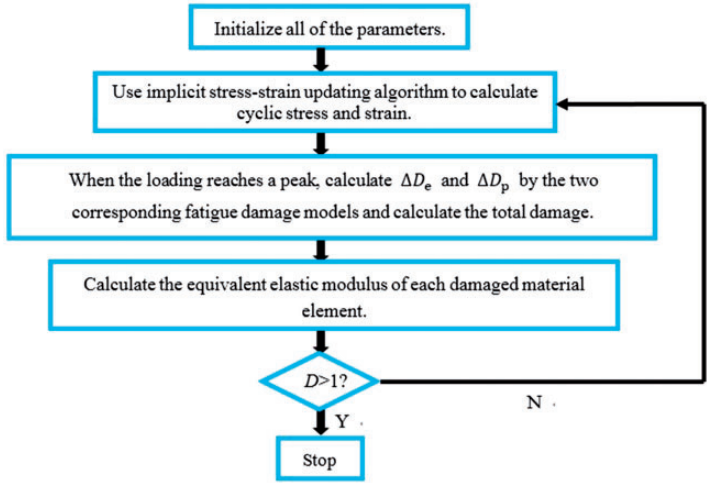

Figure 7. Numerical algorithm for fatigue damage accumulation.

(3) Calculate the increment of fatigue damage, elastic damage ΔD_e and plastic damage ΔD_p, according to the two corresponding fatigue damage models. The fatigue damage increment ΔD is assigned a maximum value of between ΔD_e and ΔD_p (Shen et al., 2015):

$$\Delta D = \max\{\Delta D_e, \Delta D_p\} \tag{28}$$

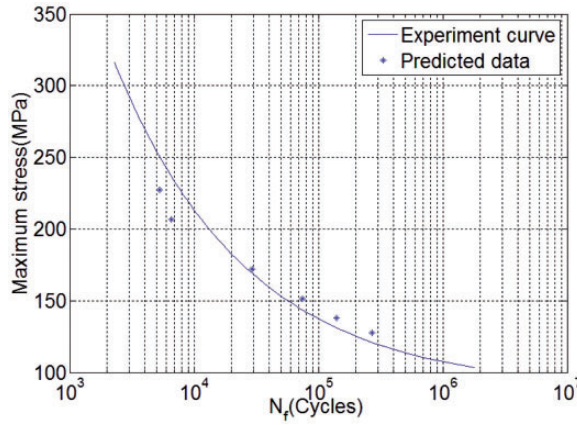

Figure 8. Comparison of the predictions with experiment data (Military Handbook-MIL-HDBK-5H, 1998) for 7075-T6 specimens.

The total damage D is calculated by

$$D^{i+1} = D^i + \Delta D^i \Delta\Delta N \tag{29}$$

where an appropriate value of ΔN is adopted in view of the computation efficiency and convergent fatigue life. In general, according to previous studies (Zhan et al., 2012, 2015), the value of ΔN is applicable when it satisfies the condition $\Delta N/N_f \leq 0.01$.

(4) Calculate the equivalent elastic modulus of each damaged material element.
(5) Repeat steps (2)–(4) until the total damage of the critical element reaches 1.

Results and discussion

Validation

To validate the calibrated material parameters and theoretical models, two groups of experimental data are used for a comparison with the predicted results. One is the experimental data of a notched specimen applied with fully reversed cyclic loading without an overload, and the other is data of a rod specimen undergoing multiple overloads and fully reversed cyclic loading.

Fatigue life of specimens under cyclic loading without overload. All fatigue experiments were carried out using a high-frequency vibrophore machine. The test frequency was between 1100 and 1500 cycles per minute. The geometry of the specimen is shown in Figure 3. The predicted life is calculated based on the numerical implementation of the fatigue damage accumulation presented in Fatigue damage accumulation section. The experiment fatigue life and predicted results are shown in Figure 8. It is clear that the predicted fatigue life is in accordance with experiment fatigue life (Military Handbook-MIL-HDBK-5H, 1998).

A variation in the cyclic stress–strain curve during fatigue can be seen in Figure 9. It shows the cyclic stress–strain curves of the critical element under fully reversed cyclic loading with a maximum

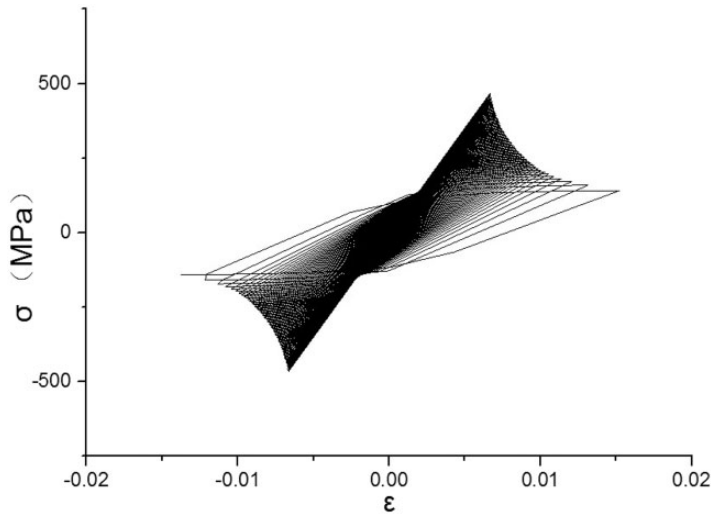

Figure 9. Cyclic stress–strain curve of the 7075-T6 specimen under fully reversed cyclic stress with $\sigma_{max} = 226.500A0MPa$.

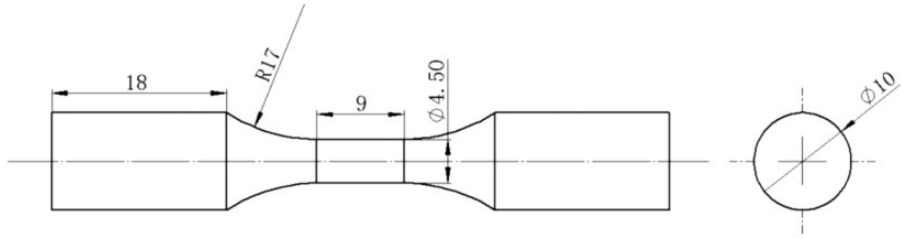

Figure 10. Dimensions (mm) of 7075 fatigue coupons (Chlistovsky et al., 2007).

stress of 226.5 MPa. It can be seen that the Young's modulus continues decreasing, while the accumulated plastic strain continues increasing along with the increase in the number of cycles.

Fatigue life of specimens under cyclic loading with multiple overloads. To validate the proposed method in predicting the fatigue life of a specimen under cyclic loading with multiple overloads, experiments were conducted based on Chlistovsky's study (Chlistovsky et al., 2007) for comparison. The material of the specimens was aluminium 7075. The geometry of the rods is shown in Figure 10 and the one-eighth finite element model of the rod is shown in Figure 11. A periodic loading spectrum containing the overloads is shown in Figure 12. Here, ΔS_{sc} indicates the difference between the maximum and minimum fatigue loads. Overloads were applied for every 200 loading cycles. The maximum fatigue load was 350 MPa. Three different values of ΔS_{sc} are described in this section.

The predicted fatigue life and experimental results (Chlistovsky et al., 2007) are listed in Table 5. The relative error of each case is around 30%. Therefore, the predicted fatigue life agrees well with the experiment data, which indicates that the proposed method can consider the effects of multiple overloads well. It is worth noting that although only 7075 aluminium alloy was used to verify the

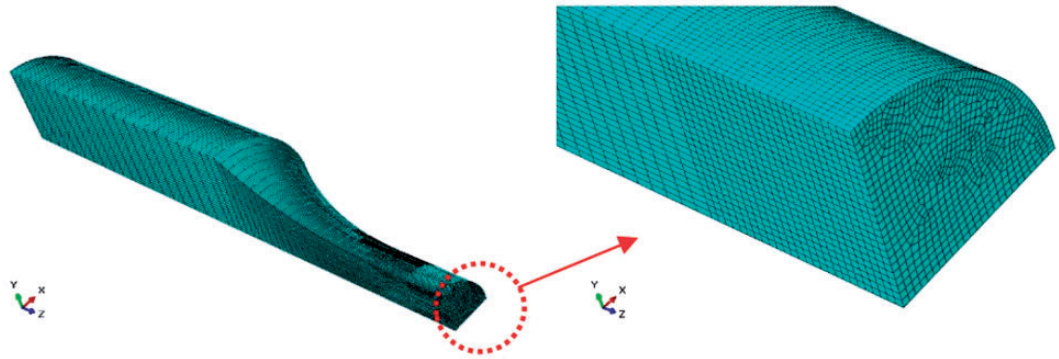

Figure 11. Finite element model of the specimen.

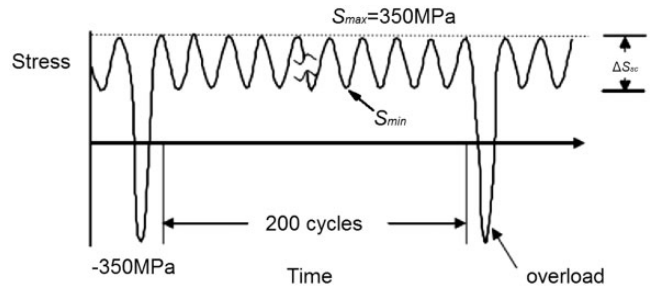

Figure 12. Periodic overload loading spectrum for 7075 aluminium alloy (Chlistovsky et al., 2007).

Table 5. Predicted fatigue life and experiment fatigue life of rods under different ΔS_{sc}.

No.	ΔS_{sc} (MPa)	Experiment fatigue life (cycles)	Predicted fatigue life (cycles)	Relative error
1	250	35,000	24,300	30.5%
2	350	24,000	15,800	34.2%
3	450	20,000	13,700	31.5%

proposed method, most of the conventional ductile metals such as aluminum alloy, steel and titanium alloy can also be applied in this method.

The following sections describe an extensive investigation of the effects of an overload from several perspectives.

Effects of single overload

To investigate the effects of a single overload, calculations on the notched specimens shown in Figure 3 under fully reversed tension-compression loadings with or without an overload were conducted, and the predicted fatigue lives are as listed in Table 6.

Table 6. Predicted life of a notched specimen under different cases.

No.	σ_{od} (MPa)	σ_{max} (MPa)	OLR	Predicted fatigue life (cycles)
1	none	205.5		6585
2	261	205.5	1.27	7285
3	270	205.5	1.31	7685
4	285	205.5	1.38	8885
5	300	205.5	1.46	9785
6	none	261		3348
7	270	261	1.03	3485
8	285	261	1.09	3585
9	300	261	1.14	3585

OLR: Overload Ratio.

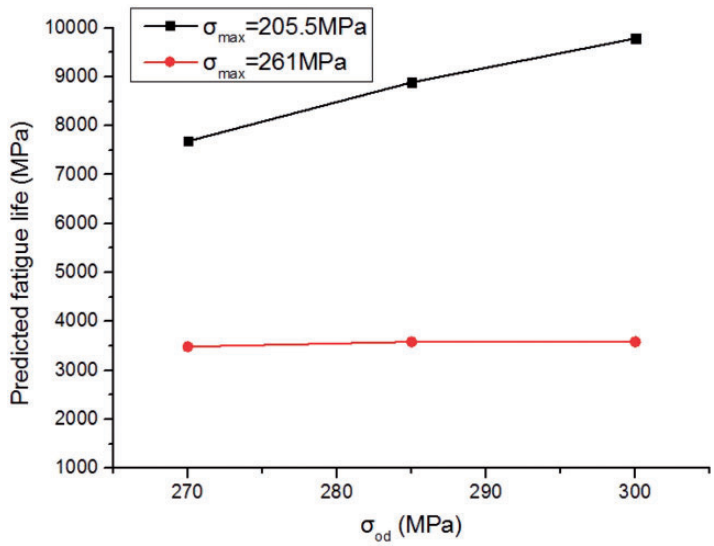

Figure 13. Predicted fatigue life under different σ_{max} and σ_{od}.

As shown in Table 6, by comparing Nos. 1–5, and Nos. 6– 9, it is clear that an overload is favourable in increasing the fatigue life. For the cases studied here, under the case of the same σ_{max}, with the increase in the overload ratio ($\sigma_{od} : \sigma_{max}$), the fatigue life continues increasing. In addition, as shown in Figure 13, by comparing the beneficial effect of an overload for the different cyclic loadings, it can seen that an overload has a more significant influence on the group with a lower stress amplitude.

Because the effects of an overload are mainly determined based on the residual stress and plastic damage, a detailed discussion of the effects of residual stress and plastic damage is provided below. In addition, the residual stress may vary during the fatigue damage evolution. Therefore, the effect of damage based on the variation in residual stress is also investigated.

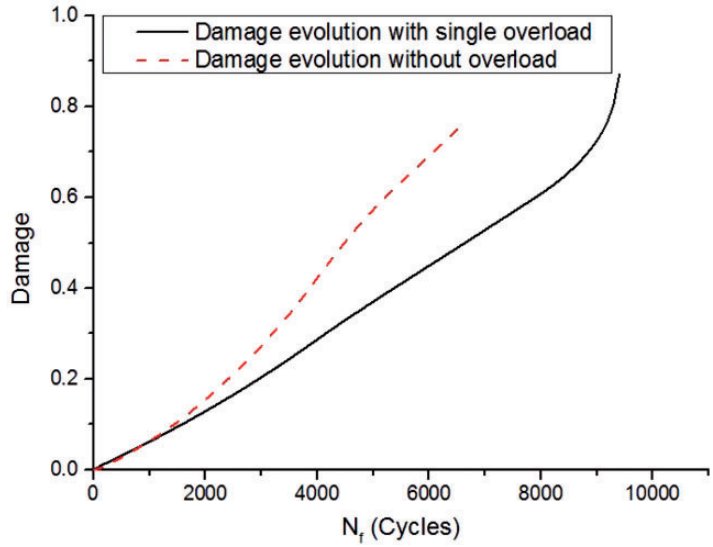

Figure 14. Damage evolution of specimens with and without overload.

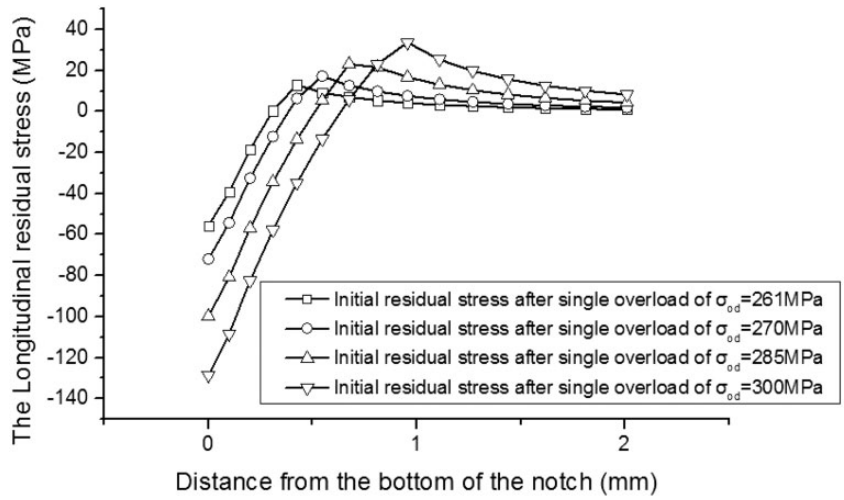

Figure 15. Initial distribution of longitudinal residual stresses with respect to the different overloads.

Effects of residual stress caused by single overload. The damage evolution in the critical element at the tip of a notch under $\sigma_{max} = 205.5$ MPa with or without an overload ($\sigma_{od} = 300$ MPa) is shown in Figure 14. For the case with an overload, the growth rate of the damage is clearly slower, which results in a longer fatigue life.

To analyse the effect of residual stress on the fatigue life, the initial longitudinal residual stresses along the depth direction away from the tip of the notch were obtained, and their distributions are as shown in Figure 15. It can be seen that the initial compressive residual stresses at the tip of the notch

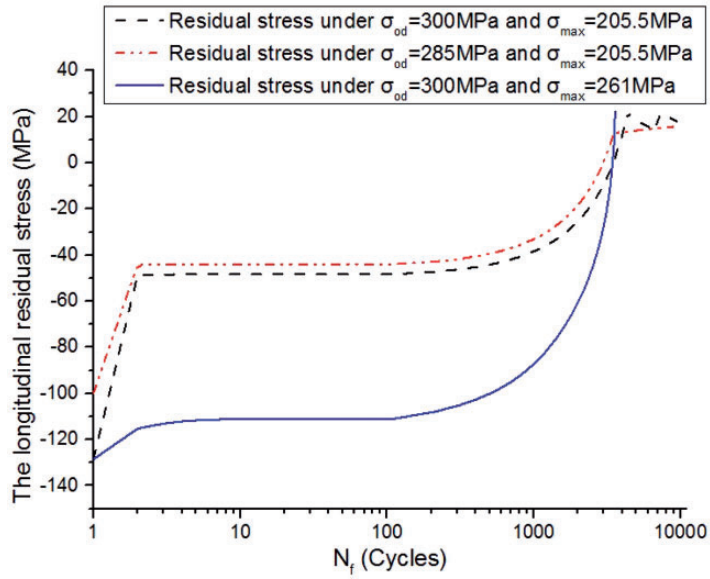

Figure 16. Relaxation of residual stress at the notch tip corresponding to the numbers of cycles of specimen applied with different σ_{od} and σ_{max}.

increase along with an increase in the overload. The superimposition of the residual stress and fatigue loading results in a decrease in the mean stress of the cyclic loading, which accordingly leads to a longer fatigue life. It can also be seen that both the maximum tensile residual stress and the compressive residual stress increase along with an increase in overload. However, the incremental magnitude of the compressive residual stress is much more remarkable, and also better explains the effect of the higher overload.

When the fatigue load is $\sigma_{max} = 261\ MPa$, the accumulated plastic strain occurs from the first loading cycle following the overload. Thus, unlike the case of low fatigue loading ($\sigma_{max} = 205.5\ MPa$, which is lower than the yield stress), the residual stress in the case of $\sigma_{max} = 261\ MPa$ changes more smoothly after an overload, and a clear knee point disappears, as shown in Figure 16. Furthermore, comparing the red line ($\sigma_{od} = 285$ MPa and $\sigma_{max} = 205.5$ MPa) and black line ($\sigma_{od} = 300$ MPa and $\sigma_{max} = 205.5$ MPa) in Figure 16, it can be concluded that the initial residual stress and the relaxed residual stress both increase when the overload ratio is greater. Meanwhile, the further relaxation of residual stress comes later for the case of a higher overload ratio, which results in a longer fatigue life than the case of a lower overload ratio.

Effects of plastic damage induced by single overload. In general, an overload causes plastic strain at the tip of the notch, and plastic damage then occurs in this area. In this section, specimens applied with different amplitudes of overload are described, and the corresponding plastic damage is calculated using equation (27).

The distributions of plastic damage caused by overloads of 285 MPa and 300 MPa are similar with that under an overload of 270 MPa (shown in Figure 6). For the three cases, the maximum plastic damage is at the notch tip. The extent of plastic damage of the critical elements, and the predicted fatigue lives considering and ignoring the initial plastic damage, are listed in Table 7. It can be seen that the maximum plastic damage becomes larger with an increase in overload, whereas

Table 7. Influence of damage on predicted life.

No.	Overload (MPa)	σ_{max} (MPa)	Predicted fatigue life (cycles)	
			With D_0	Without D_0
1	300	261	3585	3675
2	300	205.5	9785	9950
3	300	150	79,400	80,700
4	300	135	173,200	174,500
5	285	261	3585	3575
6	285	205.5	8885	8925

insignificant differences between the fatigue lives of the two groups, i.e., considering and ignoring the initial plastic damage, are shown.

It should be noted that the plastic damage is directly dependent on the plastic strain, according to equation (27). However, when the overload is too high, the value of plastic damage calculated by equation (27) will produce a remarkable error because in this study the parameters S and m are calibrated from the experiment results, with the value of ε_p caused by each loading cycle being less than 0.012. Therefore, the cases calculated in this study are only those in which plastic strains caused by an overload are less than 0.012. For a much higher level of overload, the plastic damage should be calculated by other equations or other parameter values, which will be discussed in a future study.

Effects of damage on the variation of residual stress

The stiffness of each material element continues degrading during the fatigue damage evolution, which leads to a stress redistribution in the material. The residual stress field will also vary along with an increase in the number of loading cycles. In this section, two groups of calculations are described, one of which considers the effect of the damage, whereas the other one ignores it. Specimens of both groups were applied the same tension overload and subsequent cyclic loading.

When ignoring the damage, the initial residual stress caused from a single overload decreases during the following loading cycle, and the relaxation of residual stress mainly occurs during this cycle. The relaxation of residual stress is closely related to the amplitude of the fatigue load. In general, a fatigue load with higher amplitude leads to a stronger relaxation. If the fatigue load is totally elastic, the residual stress will not change, as the line (under $\sigma_{max} = 150\,\text{MPa}$) in Figure 17 indicates.

When the damage is considered, the residual stress continues to change and does not reach a stable value. As shown in Figure 18, the relaxation of residual stress corresponding to the number of cycles is demonstrated. The entire relaxation process can be divided into four stages:

(1) Stage 1: The residual stress drastically decreases after the first loading cycle.
(2) Stage 2: The residual stress reaches a temporary stable state and remains constant. This is similar with the situation when the damage is ignored.
(3) Stage 3: The residual stress decreases again and becomes positive.
(4) State 4: The residual stress slowly turns to zero.

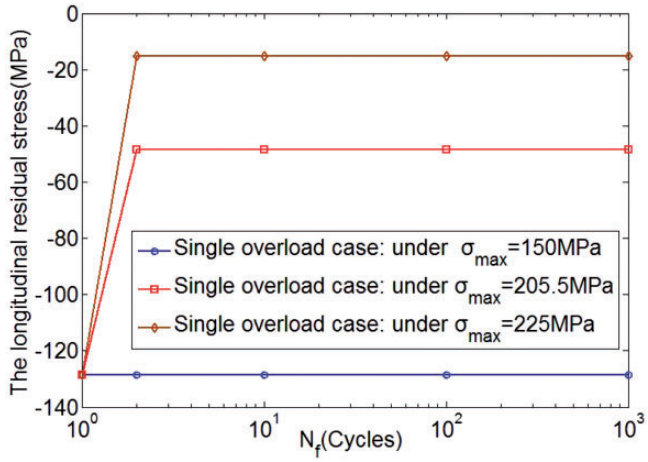

Figure 17. Relaxation of residual stress at the notch tip corresponding to the number of cycles.

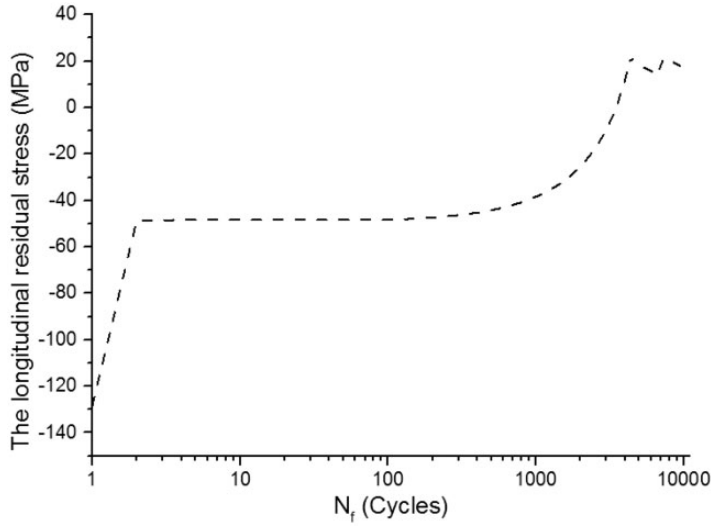

Figure 18. Relaxation of residual stress at the notch tip corresponding to the number of cycles of the specimen applied with an overload of 300 MPa and a subsequent fatigue load of $\sigma_{max} = 205.5$ MPa.

For the case shown in Figure 18, the residual stress clearly relaxes after the first loading cycle, which is due to the reversed yielding of the specimen and the occurrence of a new plastic strain. A clear knee point can then be found. Next, the residual stress remains constant, which is mainly attributed to the non-occurrence of cyclic plastic strain owing to the low stress level of the following cyclic loading. The other reason is that the damage caused by fatigue load remains small at this stage. That is, no yielding induced by damage occurs in this state. Next, as the number of cycles increases, the stiffness degradation of the material becomes increasingly serious, and a new

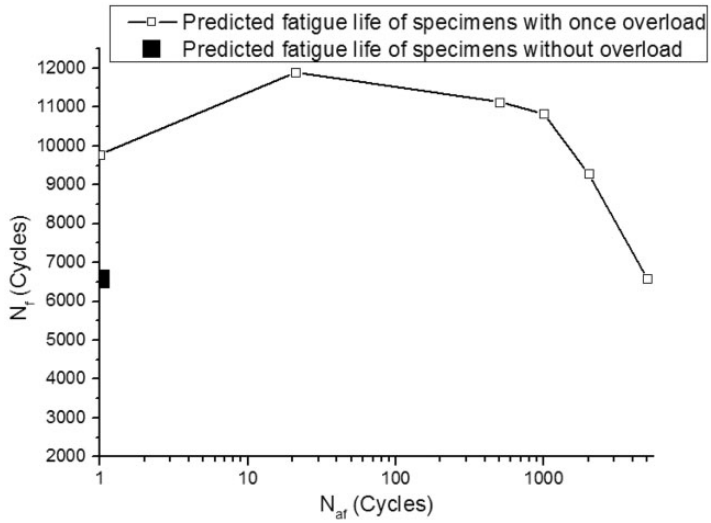

Figure 19. Fatigue life of notched specimens under $\sigma_{od} = 300$ MPa and $\sigma_{max} = 205.5$ MPa with different overload occurrence times.

accumulation of plastic strain occurs. Thus, the residual stress starts to decrease along with an increase in plastic strain at this stage. This trend is consistent with the results obtained by a previous study (Nikitin and Besel, 2008). At this stage, the residual stress continues decreasing until it develops into a positive stress from the original negative stress, although the magnitude of the residual stress remains small. Finally, in the last stage, the amount of damage is remarkable. Thus, the residual stress relaxes from a positive value to zero. Similar trends have also been found in a previous study (Nikitin and Besel, 2008).

It is clear that the fatigue damage evolution has a significant influence on the variation of residual stress. Therefore, it is necessary to take into account the coupling effects of the damage and residual relaxation to obtain a reasonable fatigue life.

Effects of occurrence time of overload. The overload exerted before the cyclic loading can significantly increase the fatigue life under the case of a relatively low fatigue load, as shown in Section 5.2. However, an overload may also be exerted after a period of cyclic loading. In this section, the effects of occurrence time of an overload (N_{af}) on the fatigue life for two cases are discussed. An overload ($\sigma_{od} = 300\ MPa$) is arranged before different numbers of loading cycles are applied. For the first case, the fatigue load is set as $\sigma_{max} = 205.5$ MPa, and N_{af} is chosen to be 1, 21, 500, 1000, 2000, and 5000. For the second case, the fatigue loading is set as 135 MPa, and N_{af} is chosen to be 1600, 9600, 28,800, 48,000, 67,200. The fatigue life of each case is predicted using the aforementioned approach.

The predicted fatigue lives of the first case are shown in Figure 19, and the curve of fatigue life versus the overload occurrence time shows a non-monotonic trend. Initially, the fatigue life increases as N_{af} increases. For the cases studied here, when N_{af} is 21, the fatigue life reaches the largest value, which is more than twice the fatigue life of the case without an overload. Then, the fatigue life slightly decreases as N_{af} increases within the range of 21–500. Thereafter, the fatigue life significantly decreases as N_{af} increases. For the second case, the trend of the fatigue life with respect to the overload occurrence time is similar with the first case. As shown in Figure 20, when $N_{af} = 28{,}800$, the

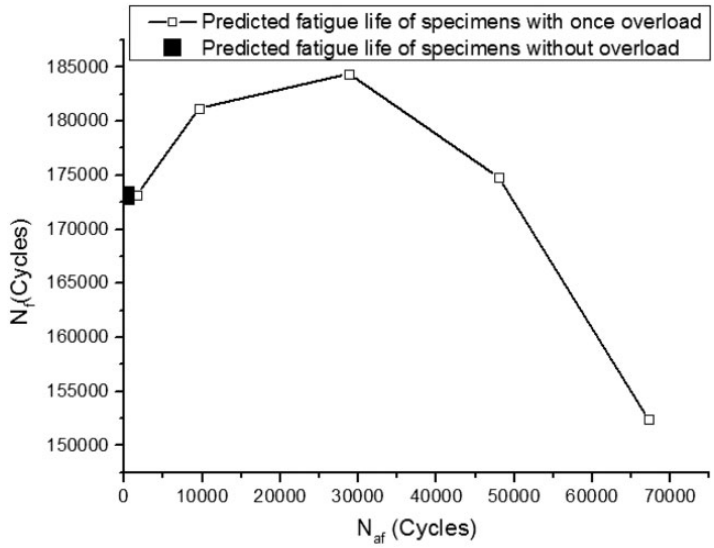

Figure 20. Fatigue life of notched specimens under $\sigma_{od} = 300$ MPa and $\sigma_{max} = 135$ MPa with different overload occurrence times.

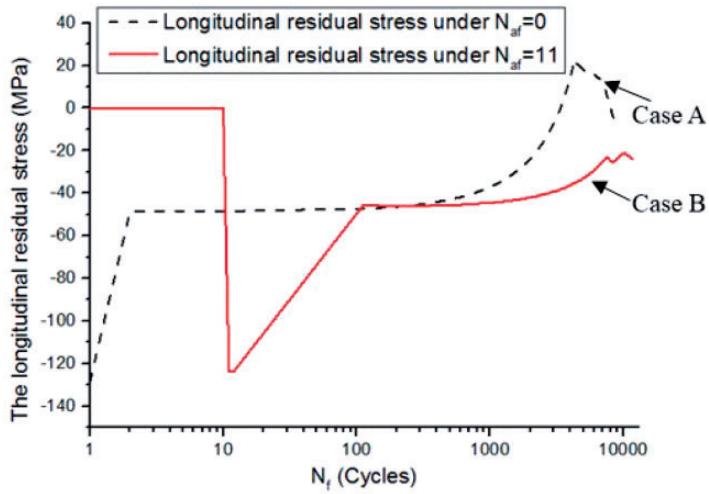

Figure 21. Longitudinal residual stress of notched specimens under $\sigma_{od} = 300$ MPa and $\sigma_{max} = 205.5$ MPa with different N_{af}.

fatigue life increases by about 12,000 cycles. This was already confirmed through different experiments (Ishihara and Mcevily, 1999), in which it was shown that exerting an overload in the middle of the loading spectrum can increase the fatigue life owing to a coaxing effect (Ishihara and Mcevily, 1999) caused by a low–high–low loading sequence.

Because the residual stress is the main factor increasing the fatigue life, the variation in residual stress for the two cases is shown in Figure 21 for the purpose of analysing the effect of the overload

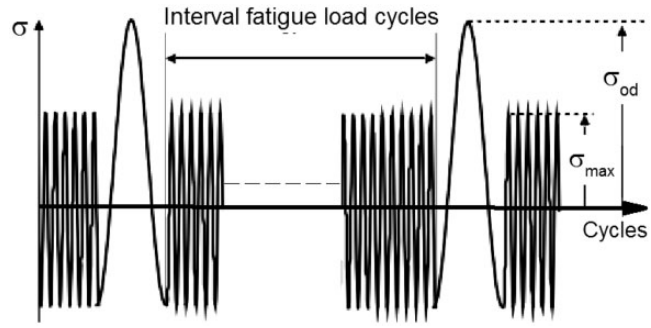

Figure 22. Load spectrum of multiple overload case.

occurrence time. As shown in Figure 21, owing to the later introduction of residual stress for case B, the relaxation process is slower, and the fatigue life is accordingly longer.

Effects of multiple overloads

When an overload is applied more than once, the effects on the fatigue life may differ. In this section, the fatigue lives of the notched specimens shown in Figure 3 undergoing multiple overloads are calculated, and the effects of the residual stress induced by multiple overloads and their occurrence frequency are described.

Effects of residual stress caused by multiple overloads. The load spectrum containing multiple overloads is illustrated in Figure 22. The notched specimens are applied an overload every 2500 loading cycles. The peak stress of the overload σ_{od} is 300 MPa, and the maximum stress of the fully reversed cyclic load is 205.5 MPa. The predicted fatigue life is 9328 cycles, which is 41.7% higher than that without an overload (case No. 1 shown in Table 6), but a little lower than that with a single overload applied before fatigue loading.

The damage evolutions of the critical element at the tip of the notch corresponding to the different cases are shown in Figure 23. In case 1, the specimen was applied a single overload before the subsequent fully reversed fatigue loading. In case 2, overloads were applied every 2500 loading cycles. The specimen in the last case simply underwent CA fatigue loading, and no overload was exerted on the specimen. On the one hand, the damage evolution rates of cases 1 and 2 are both slower than that of case 3, which means that the overloading, regardless of a single overload or multiple overloads, can decrease the damage evolution rate, and accordingly increase the fatigue life. On the other hand, as illustrated in Figure 23, during the first 2500 loading cycles, the damage evolution of cases 1 and 2 are identical because the same loading conditions were applied. After 2500 cycles, a second overload was applied in case 2, and a difference between the two cases was demonstrated, as shown in Figure 23. The damage evolution rate of case 2 is a little slower than that of case 1. However, when a third overload was applied in case 2, a jump in the damage increment was induced, thereby leading to the damage evolution rate keeping up with that of case 1. In the final phase, the damage evolution rate of case 2 is slightly greater than that of case 1, which results in a slightly shorter fatigue life. This implies that, although multiple overloads can increase the fatigue life, a proper occurrence frequency of such overloads should be determined. This issue is described in the following section.

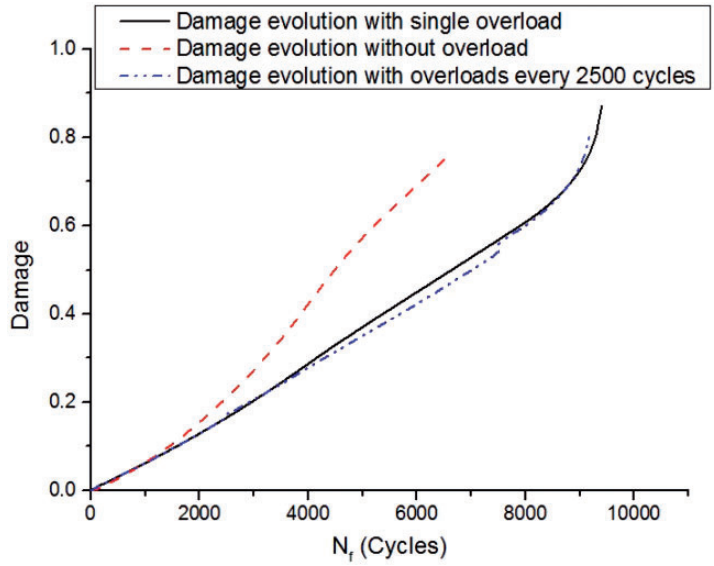

Figure 23. Damage evolution of bottom notch for different cases.

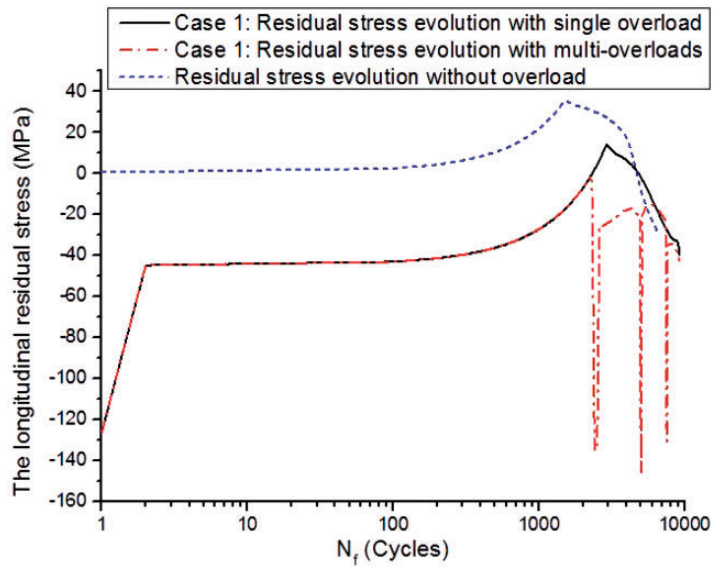

Figure 24. Evolution of longitudinal residual stress for different cases.

To investigate the different effects between a single overload and multiple overloads, the variation in longitudinal residual stress at the tip of the notch with respect to the number of cycles is presented in Figure 24. It can be seen that each overload in the case of multiple overloads induces a new residual stress, which slows down the damage evolution rate. However, at the later stage of fatigue,

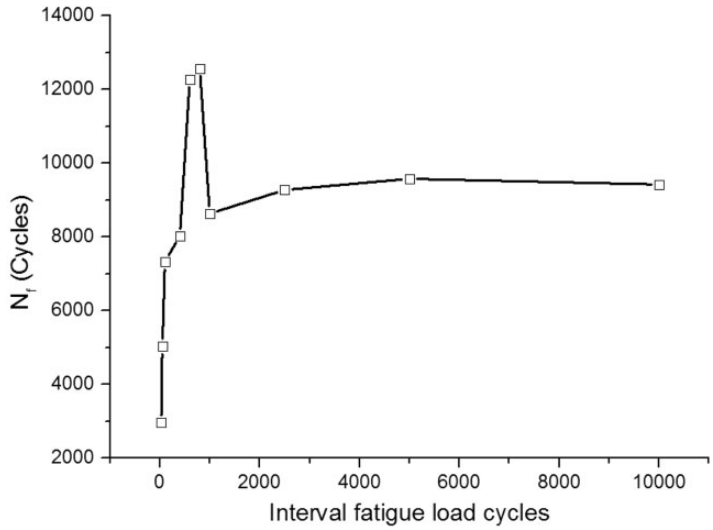

Figure 25. Fatigue life corresponding to different overload frequencies.

the benefit of this overload is wiped out by the increment of damage induced. Therefore, a positive effect is not obvious at the later stage, and a detrimental effect may even be introduced, as shown in Figure 23.

Effects of overload occurrence frequency. In this section, specimens undergoing multiple overloads with different occurrence frequencies are described. Several interval-loading cycles between two overloads were selected for two different cases. For the first case, the interval cycles are 25, 50, 100, 400, 600, 800, 1000, 2500, 5000, and 10,000 cycles. For the second case, the interval cycles are 2500, 5000, 7500, 10,000, 20,000, 30,000, 50,000, 100,000, 150,000 and 250,000 cycles. For both cases studied above, the maximum overload stress is 300 MPa, and the stress amplitude of the fatigue loading is 205.5 MPa and 135 MPa, respectively.

The predicted fatigue lives for the group in the first case corresponding to different occurrence frequencies are shown in Figure 25. The abscissa axis represents the interval cycles between overloads. It is clear that the overloads can increase the fatigue life, but when the number of interval cycles is around less than 50, the fatigue life is even lower than the case without any overloads. Thus, the overload frequency cannot be too high. It can also be inferred that when the number of interval cycles is less than 1000, the multi-overloads have a strong influence on the fatigue life. Figure 25 shows that when the number of interval cycles increases from 25 to around 700, the fatigue life rapidly increases from 2968 to the maximum value (about 12,500). The fatigue life then decreases with an increase in the number of interval cycles. After the number of interval cycles reaches greater than 1,000, the fatigue life nearly remains at a stable number of cycles, i.e., around 9500.

The predicted fatigue lives for the group in the second case corresponding to different occurrence frequencies are shown in Figure 26. When the number of interval cycles is less than 10,000, the effect of an overload on the fatigue life is clear. Then, as the number of interval cycles increases, the beneficial effect of the overloads slowly increases, and even decreases in the end.

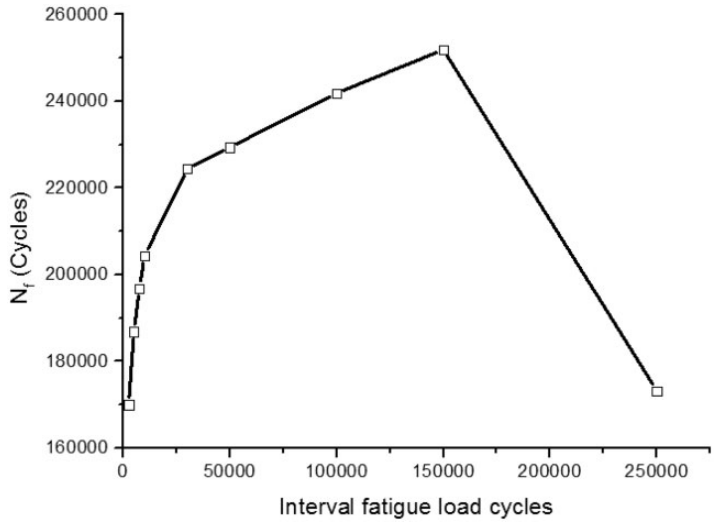

Figure 26. Fatigue life corresponding to different overload frequencies.

Conclusions

In this study, a continuum damage mechanics-based approach was proposed to analyse the effects of overloading on the fatigue life of a notched specimen by considering the residual stress and plastic damage. The relaxation of residual stress at the beginning stage, as well as the variation in residual stress along with the damage evolution of the material, was also investigated. The influences of the occurrence time of a single overload and the interval cycles between two overloads were discussed. Some of the key findings can be summarized as follows:

(1) The elastic–plastic finite element implementation is an effective method to calculate the residual stresses of a specimen. The change in fatigue life is mainly attributed to a variation in mean stress of the cyclic loading, which is induced by a superimposition of the fatigue loading and residual stresses.
(2) The damage evolution of a material has a clear effect on the relaxation behaviour of the residual stress. When damage is not considered, the residual stress decreases during the first several loading cycles and afterwards remains constant up to the failure of the specimen. However, when the damage evolution is considered, the residual stress varies with four stages: rapid relaxation, remaining constant, sluggish relaxation and attenuation to zero.
(3) For the cases studied in this paper, a single overload benefits the fatigue life of the specimen by inducing a compressive stress on the notch surface, and this compressive stress increases along with the increase in the magnitude of the overload.
(4) The occurrence time of an overload has a significant effect on the fatigue life of the specimen. The best improvement is shown when the overload is exerted after a number of loading cycles, and this beneficial effect is then reduced along with a further increase in the number of loading cycles before the overload is exerted.
(5) For cases of multiple overloads, a new residual stress field in the critical area is introduced by each overload. Accordingly, an overload has a positive effect on the fatigue life of a specimen. However, when the total accumulation of damage is large, the overload may cause a large plastic

strain, at which time, a negative effect will be induced. That is, an overload exerted during the late stage of fatigue is detrimental.

(6) The occurrence frequency of overloading has a positive effect on the fatigue life. Initially, the beneficial effect clearly increases as the number of interval cycles increases. Then, the improvement in fatigue life begins to slow along with the further increase in the number of interval cycles. Therefore, an optimum number of interval cycles exists for certain overloading and cyclic loading amounts.

Funding

The author(s) received no financial support for the research, authorship, and/or publication of this article.

References

Abdel-Karim M (2009) Modified kinematic hardening rules for simulations of ratchetting. *International Journal of Plasticity* 25: 1560–1587.

Abdel-Karim M (2010) An evaluation for several kinematic hardening rules on prediction of multiaxial stress-controlled ratchetting. *International Journal of Plasticity* 26: 711–730.

ASTM E606/E606M-12 (2012) *Standard Test Method for Strain-Controlled Fatigue Testing*. West Conshohocken, PA: ASTM international, Book of Standards Volume 03.01.

Castro JTPD, Simões DDA, Menezes IFMD, et al. (2016) A note on notch shape optimization to minimize stress concentration effects. *Theoretical & Applied Fracture Mechanics* 84: 72–85.

Chaboche JL (1986) Time-independent constitutive theories for cyclic plasticity. *International Journal of Plasticity* 2: 149–188.

Chaboche JL (1989) Constitutive equations for cyclic plasticity and cyclic viscoplasticity. *International Journal of Plasticity* 5: 247–302.

Chaboche JL (1991) On some modifications of kinematic hardening to improve the description of ratchetting effects. *International Journal of Plasticity* 7: 661–678.

Chaboche JL (2008) A review of some plasticity and viscoplasticity constitutive theories. *International Journal of Plasticity* 24: 1642–1693.

Chaudonneret M (1993) A simple and efficient multiaxial fatigue damage model for engineering applications of macro-crack initiation. *Journal of Engineering Materials & Technology* 115: 373–379.

Chengqing L, Junjun L, Tuo L, et al. (2013) Theoretical calculation and numerical simulation on residual stress after unloading in the plastic phase. *Building Structures* 2: 441–444.

Chlistovsky RM, Heffernan PJ and Duquesnay DL (2007) Corrosion-fatigue behaviour of 7075-T651 aluminum alloy subjected to periodic overloads. *International Journal of Fatigue* 29: 1941–1949.

Dalaei K and Karlsson B (2011) Influence of overloading on fatigue durability and stability of residual stresses in shot peened normalized steel. *Materials Science & Engineering A* 528: 7323–7330.

Darban H, Nosrati M and Djavanroodi F (2014) Multiaxial fatigue analysis of stranded-wire helical springs. *International Journal of Damage Mechanics* 24: 1361–1364.

Dowling NE (1993) *Mechanical Behavior of Materials: Engineering Methods for Deformation, Fracture, and Fatigue*. New York: Prentice Hall, p. 59.

Gallagher JP (1974) A generalized development of yield zone models. *A Generalized Development of Yield Zone Models* No. Affdl-Tm-Fbr-74-28. Air Force Flight Dynamics Lab Wright-Patterson Afb Oh.

Ishihara S and Mcevily AJ (1999) Coaxing effect in the small fatigue crack growth regime. *Scripta Materialia* 42: 617–622.

Kauzlarich JJ (1989) The Palmgren-Miner rule derived. *Tribology* 14: 175–179.

Lemaître JJ (1992) *A Course on Damage Mechanics*. Heidelberg: Springer Berlin, pp. 1–37.

Lemaitre J, Chaboche JL and Maji AK (1993) Mechanics of solid materials. *Journal of Engineering Mechanics* 119: 642–643.

Lemaitre J and Desmorat R (2005) *Engineering Damage Mechanics*. Heidelberg: Springer Berlin.

Lv Z, Huang HZ, Zhu SP, et al. (2015) A modified nonlinear fatigue damage accumulation model. *International Journal of Damage Mechanics* 24: 168–181.

Military Handbook-MIL-HDBK-5H (1998) *Metallic Materials and Elements for Aerospace Vehicle Structures*. New York: Knovel Interactive Edition, US Department of Defense.

Nikitin I and Besel M (2008) Residual stress relaxation of deep-rolled austenitic steel. *Scripta Materialia* 58: 239–242.

Ramos MS, Pereira MV, Darwish FA, et al. (2003) Effect of single and multiple overloading on the residual fatigue life of a structural steel. *Fatigue & Fracture of Engineering Materials & Structures* 26: 115–121.

Sander M and Richard HA (2005) Finite element analysis of fatigue crack growth with interspersed mode I and mixed mode overloads. *International Journal of Fatigue* 27: 905–913.

Sarkheil S and Foumani MS (2014) Numerical and experimental study on the optimization of overload parameters for the increase of fatigue life. *Aerospace Science & Technology* 35: 80–86.

Shen F, Hu W and Meng Q (2016) A non-local approach based on the hypothesis of damage dissipation potential equivalence to the effect of stress gradient in fretting fatigue. *International Journal of Fatigue* 90: 125–138.

Shen F, Hu W, Voyiadjis GZ, et al. (2015) Effects of fatigue damage and wear on fretting fatigue under partial slip condition. *Wear* 338–339: 394–405.

Shen F, Voyiadjis GZ, Hu W, et al. (2015) Analysis on the fatigue damage evolution of notched specimens with consideration of cyclic plasticity. *Fatigue & Fracture of Engineering Materials & Structures* 38: 1194–1208.

Smith MC, Bouchard PJ and Turski M (2012) Accurate prediction of residual stress in stainless steel welds. *Computational Materials Science* 54: 312–328.

Sun Y, Voyiadjis GZ, Hu W, et al. (2017) Fatigue and fretting fatigue life prediction of double-lap bolted joints using continuum damage mechanics-based approach. *International Journal of Damage Mechanics* 26(1): 162–188.

Suresh S and Giannakopoulos AE (1998) A new method for estimating residual stresses by instrumented sharp indentation. *Acta Materialia* 46: 5755–5767.

Theil N (2016) Fatigue life prediction method for the practical engineering use taking in account the effect of the overload blocks. *International Journal of Fatigue* 90: 23–35.

Walker EK (1970) The effect of stress ratio during crack propagation and fatigue for 2024-T3 and 7075-T6 aluminum. *Effects of environment and complex load history on fatigue life*. ASTM International.

Warhadpande A, Sadeghi F, Kotzalas MN, et al. (2012) Effects of plasticity on subsurface initiated spalling in rolling contact fatigue. *International Journal of Fatigue* 36: 80–95.

Xiao L, Ye D, Chen C, et al. (2014) Instrumented indentation measurements of residual stresses around a crack tip under single tensile overloads. *International Journal of Mechanical Sciences* 78: 44–51.

Zghal J, Gmati H, Mareau C, et al. (2016) A crystal plasticity based approach for the modelling of high cycle fatigue damage in metallic materials. *International Journal of Damage Mechanics* 25: 611–628.

Zhang T, Mchugh PE and Leen SB (2012) Finite element implementation of multiaxial continuum damage mechanics for plain and fretting fatigue. *International Journal of Fatigue* 44: 260–272.

Zhan Z, Hu W, Zhang M, et al. (2015a) The fatigue life prediction for structure with surface scratch considering cutting residual stress, initial plasticity damage and fatigue damage. *International Journal of Fatigue* 74: 173–182.

Zhan Z, Hu W, Meng Q, et al. (2015b) Continuum damage mechanics-based approach to the fatigue life prediction for 7050-T7451 aluminum alloy with impact pit. *International Journal of Damage Mechanics* 25: 943–966.

Zuo FJ, Huang HZ, Zhu SP, et al. (2015) Fatigue life prediction under variable amplitude loading using a nonlinear damage accumulation model. *International Journal of Damage Mechanics* 24(5): 767–784.